Enhanced diffusion upon amorphous-to-nanocrystalline phase transition in $Mo/B_4C/Si$ layered systems

V. I. T. A. de Rooij-Lohmann,[1,a)] A. E. Yakshin,[1] R. W. E. van de Kruijs,[1] E. Zoethout,[1] A. W. Kleyn,[1] E. G. Keim,[2] M. Gorgoi,[3] F. Schäfers,[3] H. H. Brongersma,[4] and F. Bijkerk[1,2]
[1]*FOM Institute for Plasma Physics Rijnhuizen, P.O. Box 1207, 3430 BE Nieuwegein, The Netherlands*
[2]*MESA+ Institute for Nanotechnology, University of Twente, P.O. Box 217, 7500 AE Enschede, The Netherlands*
[3]*Helmholtz-Zentrum Berlin für Materialien und Energie GmbH, BESSY II, Albert-Einstein Straße 15, 12489 Berlin, Germany*
[4]*Tascon GmbH, Heisenbergstraße 15, 48149 Münster, Germany*

(Received 29 March 2010; accepted 5 June 2010; published online 15 July 2010)

The effect of an amorphous-to-nanocrystalline phase transition on the diffusion across an interface layer of subnanometer thickness has been investigated in real-time. The diffusion in the $Mo/B_4C/Si$ thin film structure studied was found to instantaneously enhance by an order of magnitude upon the formation of nanocrystals inducing the atomic-scale onset of grain boundary diffusion. © *2010 American Institute of Physics*. [doi:10.1063/1.3460107]

I. INTRODUCTION

Diffusion at the nanometer-scale is a vast research field in microelectronics, optics, and thin film physics in general. The influence of the materials' morphology (amorphous, nanocrystalline, microcrystalline) on the diffusion rate is widely recognized and the comparison between diffusion through amorphous and crystalline layers has been the subject of several investigations.[1,2] Amorphous-to-polycrystalline transitions are regularly observed in thin film systems, once the film reaches a certain temperature or thickness. This transition can be expected to increase the diffusion rate by enabling an additional diffusion mechanism to interstitial or substitutional diffusion, namely, grain boundary diffusion (see, e.g., Ref. 3). This paper reports on the interplay between morphology and diffusion processes at the subnanometer scale using several state-of-the-art analysis techniques, and includes evidence of a crystalline transition directly causing accelerated diffusion across an interlayer.

A $Mo/B_4C/Si$ layered system is selected for this study as a typical example of current thin film research. It is applied in modern multilayer reflective optics where diffusion damages the layered structure and limits the performance.[4] While Mo and Si are selected for their favorable optical constants, the role of B_4C is to reduce interdiffusion of Mo and Si. The system shows an amorphous-to-nanocrystalline transition when the $MoSi_2$ interface that forms upon diffusion reaches a certain critical thickness.[5] We will show in this paper that this crystallization of the interface brings about an instantaneous increase in the diffusion rate by up to one order of magnitude.

II. DIFFUSION RATE

A. Experimental details

The $Mo/B_4C/Si$ trilayered structures have been prepared using physical vapor (electron-beam) deposition. The UHV deposition facility was described in detail in Ref. 6. The base pressure was lower than 2×10^{-8} mbar. A set of three quartz crystal microbalances controlled the film thickness. The deposition rate was 0.02 nm/s for Mo and 0.03 nm/s for B_4C and Si. The samples consisted of 10.0 nm c-Mo/d_{B_4C} B_4C/5.0 nm a-Si trilayers, deposited onto superpolished silicon wafer substrates at room temperature. Deposition flux masking was implemented during B_4C deposition, yielding samples with varying B_4C thickness $d_{B_4C}=0-1.6$ nm in a single coating run, ensuring identical conditions for all samples. The samples were annealed at 500 °C (systematic error <30 °C, reproducibility <2 °C). This temperature was reached 40–50 s after switching on the heating filament and was monitored with an Impac 140 pyrometer.

To investigate the diffusion process with the high time-resolution of 1 min, we performed high-sensitivity low energy ion spectroscopy (LEIS) measurements both before and during the annealing treatment. Using a recently proposed procedure,[7] these measurements provided us with the Mo concentration profile. Combining this concentration profile with Fick's second law yielded the diffusion-related quantity $\sqrt{Dt}$, where D denotes the diffusion coefficient and t the annealing time. Reference 7 describes the procedure to obtain $\sqrt{Dt}$ from a LEIS spectrum in detail. The procedure requires that the main diffusing species and the stoichiometry of the formed compound are known. Following a study of the Mo/Si system reported in Ref. 8, the main diffusing species was assumed to be Si, while the predominantly formed compound was $MoSi_2$.[7,9,10] The extraction of $\sqrt{Dt}$ further requires knowledge of the He stopping powers in B_4C (S_{B_4C}) and in Si ($S_{Si}=36\pm3$ eV/nm).[7] $S_{B_4C}=(54\pm3)$ eV/nm was es-

a)Electronic mail: v.i.t.a.derooij@rijnhuizen.nl.

 © 2010 American Institute of Physics

Downloaded 21 Dec 2010 to 130.89.85.158. Redistribution subject to AIP license or copyright; see http://jap.aip.org/about/rights_and_permissions

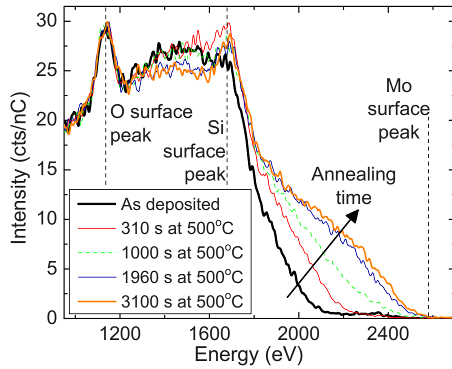

FIG. 1. (Color online) The evolution of the LEIS spectrum of the Mo/B_4C/Si sample with $d_{B_4C}=1.3$ nm, during annealing at 500 °C.

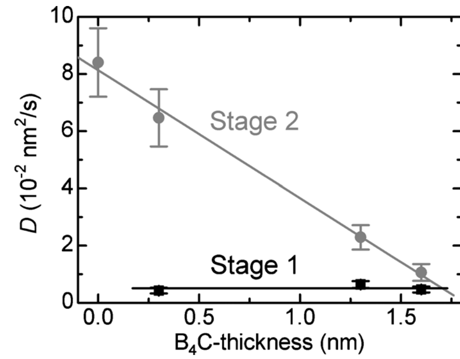

FIG. 3. The diffusion coefficient D in Stages 1 and 2, as a function of B_4C interlayer thickness d_{B_4C}.

tablished following the procedure in Ref. 7. The LEIS measurements were performed using a 3 keV He^+ beam and the Calipso LEIS instrument, which was described in detail by Brongersma *et al.*[11,12] The high sensitivity of this instrument allows reduction in the ion dose to a level below the detection limit of ion-induced sputtering or intermixing.

B. Results

As an example, Fig. 1 displays the evolution of the LEIS spectrum of a sample with $d_{B_4C}=1.3$ nm upon annealing at 500 °C. The changes in the 1850–2580 eV range are evident as follows: the onset shifts to a higher energy, and the intensity increases. In the absence of other heavy elements, that range could be uniquely attributed to Mo. The changes thus reflect the buried Mo effectively moving toward the sample surface as a result of the downward diffusion of Si. At energies below 1850 eV however, various lighter elements (Si, O, C, B) contribute to the signal and make it impossible to attribute it to a specific element. As such, only the Mo-related, high energy part of the spectrum (>1850 eV) is considered in detail.

Figure 2 shows the evolution of $\sqrt{Dt}$ for four samples with different d_{B_4C}, as obtained from quantification of the LEIS spectra of samples with varying d_{B_4C}. Without B_4C interlayer, the diffusion obeyed Fick's second law until $t=350$ s, with $D=(8.4\pm1.2)\times10^{-20}$ m^2/s. This value is

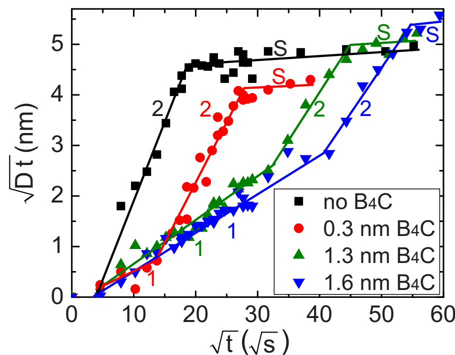

FIG. 2. (Color online) $\sqrt{Dt}$, the quantity obtained from applying Fick's law to the quantified LEIS spectra of four samples with different d_{B_4C}, plotted as a function of $\sqrt{t}$. The lines represent the best linear fit for the corresponding part of the graph and their slope represents $\sqrt{D}$. The encapsulated numbers indicate the diffusion stage (an S indicates steady state).

comparable to literature values for the Mo/Si system.[8,13] B_4C is known to reduce the diffusion rate in Mo/Si structures,[14] and adding a B_4C-layer indeed initially slowed down the diffusion to $D=(5\pm1)\times10^{-21}$ m^2/s, regardless of d_{B_4C}. We call this Stage 1. At a certain moment, however, a remarkable transition to an up to fifteen times faster regime (Stage 2) was observed. Finally, an apparent steady state (i.e., no changes observed at a timescale of an hour) is reached. Figure 3 displays D in Stage 1 and 2 as a function of d_{B_4C}. It shows that $D_{\text{Stage 1}}$ is independent of d_{B_4C} (the duration of Stage 1 increases though for thicker d_{B_4C}), while $D_{\text{Stage 2}}$ reduces linearly with increasing d_{B_4C}.

III. CHEMISTRY

In explaining the peculiar enhancement of the diffusion in Stage 2, the morphology of the structure will be investigated. Beforehand, however, we will study the chemical processes upon annealing and exclude that the system's chemistry plays a decisive role before investigating the morphology of the structure: in view of reported B_4C decomposition and MoB_x formation,[15] it is conceivable that a chemical reaction between Mo, Si, and B_4C brings about the following two-stage process: upon entering the B_4C layer, the diffusant is trapped in a chemical bond, e.g., MoB_x or SiC_x. During Stage 1, the chemical trapping would slow down the diffusion, until Stage 1 ends when the complete B_4C layer is consumed. In Stage 2, the faster process of unhindered physical diffusion would take over.

A. Experimental details

The chemical reactivity of the interface and particularly its role in relationship with the two-stage process was investigated with hard x-ray photoelectron spectroscopy (HAXPES). Compared to conventional x-ray photoelectron spectroscopy (XPS), HAXPES takes advantage of a higher x-ray energy, which increases the inelastic mean free path of the photoelectrons from typically 2.5 nm (XPS at 1486.6 eV) to 3.5 nm–6 nm (HAXPES at 2010 eV and 4020 eV, respectively). This allowed us to investigate an interface buried at a depth of 5 nm nondestructively. The HAXPES measurements have been performed at the "HIKE" experimental station[16] at the KMC-1 beamline[17] of the storage ring facility BESSY II. Samples with 1.3 nm B_4C, prepared using various annealing

Downloaded 21 Dec 2010 to 130.89.85.158. Redistribution subject to AIP license or copyright; see http://jap.aip.org/about/rights_and_permissions

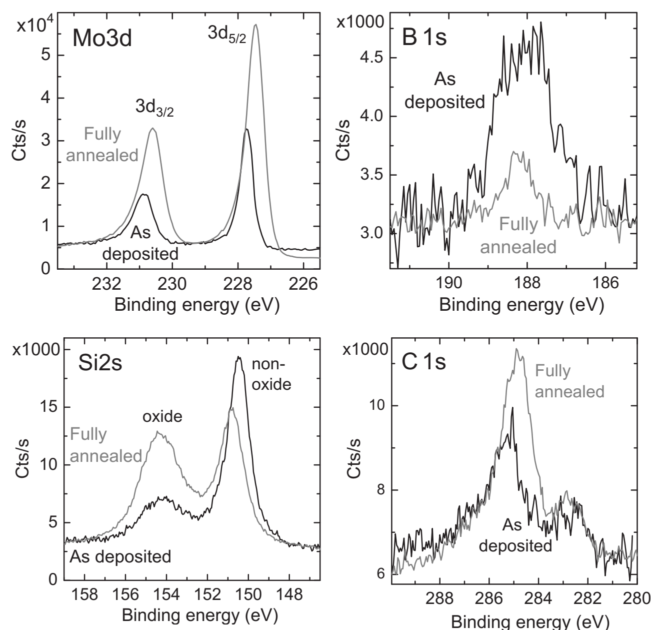

FIG. 4. The Mo 3d, Si 2s, B 1s, and C 1s HAXPES spectra of both the as deposited and the fully annealed ($\sqrt{t}=53$ $s^{1/2}$; steady state) sample with 1.3 nm B_4C. All spectra were acquired with an incident photon energy of 2010 eV.

times at 500 °C, were first characterized with LEIS and subsequently investigated with HAXPES. The Si 2s, Mo 3d, O 1s, B 1s, and C 1s peaks were measured using a Si (111) double crystal monochromator and an incident photon energy of 2010 and 4020 eV.

B. Results

Figure 4 shows the Si 2s, Mo 3d, B 1s, and C 1s peaks taken from the *as deposited* sample ($t_{B_4C}=1.3$ nm; $\sqrt{t}=0$ $s^{1/2}$) and a sample that had been annealed till steady state ($t_{B_4C}=1.3$ nm; $\sqrt{t}=53$ $s^{1/2}$), as measured with a photon energy of 2010 eV. The Si 2s peak at 154 eV corresponds to oxidized Si from the native oxide at the sample surface. Because SiO_2 is stable at our annealing temperature,[7,18] only the nonoxide silicon peak at 150.5 eV is discussed below. The increase in Mo 3d:Si 2s ratio upon annealing confirms the increased near-surface presence of Mo that resulted from Si diffusing downwards into Mo. Additionally, clear shifts in

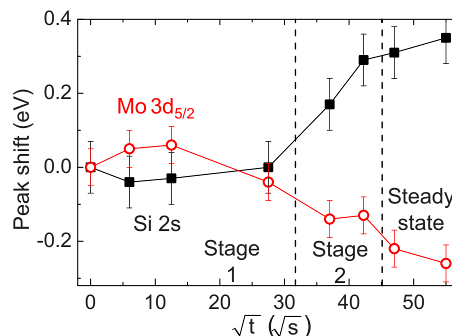

FIG. 6. (Color online) The peak shifts in the Mo $3d_{5/2}$ and the Si 2s peaks as a function of the annealing time, as measured for the Mo/1.3 nm B_4C/Si sample with an x-ray energy of 2010 eV. The dashed lines indicate the times for which changes in diffusion rate were observed with LEIS.

the Mo $3d_{5/2}$ (−0.26 eV, in accordance with a $MoSi_2$-induced shift[19]) and Si 2s peaks (+0.35 eV) indicate compound formation. Figure 5 presents the evolution of the widths of several peaks, but only marginal changes are observed for the Si 2s and the Mo $3d_{5/2}$ peak widths. The evolution of the peaks shifts, shown in Fig. 6, on the contrary, show that the chemical process of $MoSi_2$ formation speeds up at the onset of the faster Stage 2.

The C 1s spectrum in Fig. 4 comprises two peaks: one at 285 eV and the other one at 282.5 eV. Since the C signal at 285 eV is generally associated with (hydrocarbon) contamination at the sample surface, we will only consider the peak at 282.5 eV, which is associated with carbides. As the amount of deposited carbon is very small, changes in the peak width or position of this C 1s peak were below the measurement error. The C concentration as a function of annealing time though are displayed in Fig. 7. Since the C concentration does not change within the measurement accuracy, the question remains whether the carbon stayed at the interface or has diffused in both directions: into Si as well as into Mo.

Figures 4 and 7 further show that the B 1s concentration diminished by as much as a factor of 6, thus clearly suggesting that B has diffused downwards, viz., away from Si, toward Mo, evidently forming predominantly MoB_x. After a sharp drop in the beginning of the annealing, the B concentration (Fig. 7) continued to decrease gradually, therewith

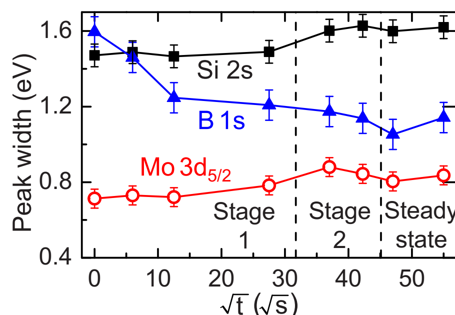

FIG. 5. (Color online) The width of the Si 2s, B 1s, and Mo $3d_{5/2}$ peaks of the Mo/1.3 nm B_4C/Si sample as a function of the annealing time. The x-ray energy was 4020 eV. The dashed lines indicate the times for which changes in diffusion rate were observed with LEIS.

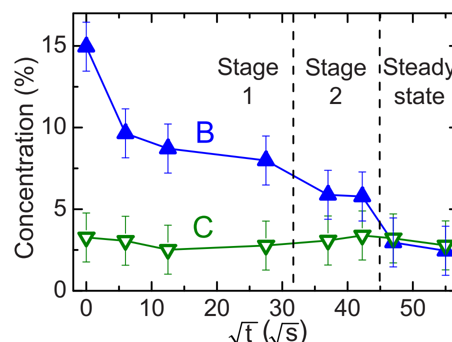

FIG. 7. (Color online) The B (squares) and C (open circles) concentrations of the Mo/1.3 nm B_4C/Si sample as a function of the annealing time, as determined from the B 1s and the C 1s (at 282.5 eV) HAXPES peaks, respectively. The measurements are performed at 2010 eV.

Downloaded 21 Dec 2010 to 130.89.85.158. Redistribution subject to AIP license or copyright; see http://jap.aip.org/about/rights_and_permissions

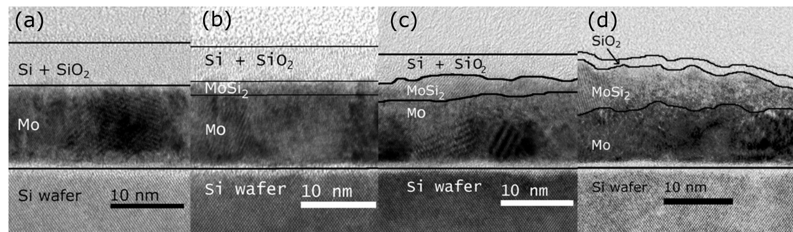

FIG. 8. TEM images of Mo/1.3 nm B_4C/Si samples in different annealing states. (a) $\sqrt{t}=0\ s^{1/2}$; (b) $\sqrt{t}=27\ s^{1/2}$; (c) $\sqrt{t}=37\ s^{1/2}$; and (d) $\sqrt{t}=53\ s^{1/2}$. The B_4C layer is too thin and its contrast too small to be visible in the TEM images. The SiO_2 is not distinguishable from the Si layer and is therefore only indicated separately in (d), where the Si layer has been completely consumed by $MoSi_2$ formation.

strongly suggesting that B first diffused into the Mo layer to form MoB_x, then continued to diffuse downwards. Figures 4 and 5 show that the B 1*s* peak has also become narrower, which provides further proof that B is chemically active and that the B_4C decomposes upon annealing. More importantly, the B 1*s* peak width has reduced to its final width already after $\sqrt{t}=12\ s^{1/2}$, indicating that all B_4C has decomposed already well before the transition to Stage 2. In contrast, at the transition point to Stage 2 no significant chemical changes were observed that can explain the acceleration of the diffusion. Hence, a chemical process is excluded as the cause for the acceleration of the diffusion, leaving it to be explained by a change in the morphology.

IV. MORPHOLOGY

A. Experimental details

After ruling out the chemical changes involving B or C at the interface as the cause for the change in diffusion rate, we investigated the evolution of the morphology of the samples and its role in the enhancement of the diffusion rate. A Philips CM300ST-FEG (scanning) transmission electron microscopy ((S)TEM) instrument was utilized to analyze several cross-sectional TEM specimens before and after the transition point from Stage 1 to Stage 2 (Fig. 2). The TEM specimens were prepared according to the procedure described in Ref. 20. The images were recorded with a magnification of 2.7×10^5 and an acceleration voltage of 300 kV.

B. Results

Figure 8 displays TEM images of samples with $d_{B_4C}=1.3$ nm in various diffusion states ($\sqrt{t}=0\ s^{1/2}$, 27 $s^{1/2}$, 37 $s^{1/2}$, and 53 $s^{1/2}$, respectively). Amorphous Si and polycrystalline Mo layers were observed in all the structures regardless of their annealing state. Note that the B_4C layer is too thin and its contrast too small to be visible in the TEM images. Before annealing, the layers were smooth and uniform. After annealing ($\sqrt{t}=53\ s^{1/2}$), however, a polycrystalline $MoSi_2$ layer has developed, as well as layer thickness variations in as much as 4 nm.

The transition from diffusion Stage 1 to the faster Stage 2 occurs at $\sqrt{t}=32\ s^{1/2}$, i.e., in between Figs. 8(b) and 8(c). A clear change in the morphology of the interface is observed exactly at that point: the interface was amorphous before the transition, while crystallites of 10–15 by 3 nm are seen afterwards. The concurrence of the crystallization and the transition to Stage 2 confirms that crystallization at the interfaces is the cause of the following abrupt increase in diffusion speed: when the amorphous structure turned polycrystalline, grain boundaries were created and these imperfections are known to act as preferential pathways and accelerators for diffusion.[21] Moreover, grain boundary diffusion is presumably also the cause of the development of layer thickness variations, as it is an inhomogeneous process by nature.

Recalling the decomposition of B_4C at an early stage and the dependence of the transition point on d_{B_4C}, we conclude that, at 500 °C, the barrier function of B_4C mainly lies in the crystallization-retarding action of B and/or C. A similar action has been reported in Ref. 22. The linear decrease in $D_{\mathrm{Stage\ 2}}$ with increasing d_{B_4C} in Fig. 2 further indicates that, *after* the crystallization, the diffusion rate is decreased by B and/or C. No such dependence is observed *before* the crystallization, which suggests that the crystallite size, and consequently D, is affected by the B or C concentration.

V. CONCLUSION

In conclusion, we have studied diffusion in $Mo/B_4C/Si$ trilayer thin film systems with subnanometer resolution to investigate the effect of the amorphous-to-nanocrystalline transition on the diffusion rate. We found that the diffusion occurred in two distinct stages before reaching a steady state. Stage 1 is characterized by relatively slow diffusion obeying Fick's second law, while Stage 2 is marked by an increased diffusion rate. The appearance of nanocrystalline regions at the interfaces proves that the increased diffusion rate is directly caused by the amorphous-to-nanocrystalline transition followed by enhanced diffusion along the grain boundaries of the crystallites. It was excluded that decomposition of the B_4C barrier and formation of molybdenum boride caused the enhanced diffusion. The B_4C interlayer increases the duration of Stage 1, due to B and/or C acting as crystallization-retarding agents. Stage 2 ends when all available Si has been transformed into the silicide, and a steady state is reached.

ACKNOWLEDGMENTS

This work is part of the FOM Industrial Partnership Programme I10 (XMO) which is carried out under contract with Carl Zeiss SMT AG, Oberkochen and the "Stichting voor Fundamenteel Onderzoek der Materie (FOM)," the latter being financially supported by the "Nederlandse Organisatie voor Wetenschappelijk Onderzoek (NWO)." The HAXPES measurements were supported by the European Community-Research Infrastructure Action under the FP6 "Structuring

Downloaded 21 Dec 2010 to 130.89.85.158. Redistribution subject to AIP license or copyright; see http://jap.aip.org/about/rights_and_permissions

the European Research Area" Programme (through the Integrated Infrastructure Initiative" Integrating Activity on Synchrotron and Free Electron Laser Science-Contract No. R II 3-CT-2004-506008).

[1]S. Mirabella, D. De Salvador, E. Bruno, E. Napolitani, E. F. Pecora, S. Boninelli, and F. Priolo, Phys. Rev. Lett. **100**, 155901 (2008).
[2]R. Winter and P. Heitjans, J. Phys. Chem. B **105**, 6108 (2001).
[3]A. Lakatos, A. Csik, G. A. Langer, G. Erdelyi, G. L. Katona, L. Daroczi, K. Vad, J. Toth, and D. L. Beke, Vacuum **84**, 130 (2009).
[4]S. P. Hau-Riege, H. N. Chapman, J. Krzywinski, R. Sobierajski, S. Bajt, R. A. London, M. Bergh, C. Caleman, R. Nietubyc, L. Juha, J. Kuba, E. Spiller, S. Baker, R. Bionta, K. S. Tinten, N. Stojanovic, B. Kjornrattanawanich, E. Gullikson, E. Plönjes, S. Toleikis, and T. Tschentscher, Phys. Rev. Lett. **98**, 145502 (2007).
[5]I. Nedelcu, R. W. E. van de Kruijs, A. E. Yakshin, and F. Bijkerk, Phys. Rev. B **76**, 245404 (2007).
[6]S. Bruijn, R. W. E. van de Kruijs, A. E. Yakshin, and F. Bijkerk, Defect Diffus. Forum **283-286**, 657 (2009).
[7]V. I. T. A. de Rooij-Lohmann, A. W. Kleyn, F. Bijkerk, H. H. Brongersma, and A. E. Yakshin, Appl. Phys. Lett. **94**, 063107 (2009).
[8]M. Salamon and H. Mehrer, Z. Metallk. **96**, 833 (2005).
[9]P. Reinig, F. Fenske, W. Fuhs, A. Schöpke, and B. Selle, Appl. Surf. Sci. **210**, 301 (2003).
[10]C. M. Doland and R. J. Nemanich, J. Mater. Res. **5**, 2854 (1990).
[11]H. H. Brongersma, M. Draxler, M. de Ridder, and P. Bauer, Surf. Sci. Rep. **62**, 63 (2007).
[12]M. Draxler, R. Gruber, H. H. Brongersma, and P. Bauer, Phys. Rev. Lett. **89**, 263201 (2002).
[13]K. Holloway, K. B. Do, and R. Sinclair, J. Appl. Phys. **65**, 474 (1989).
[14]T. Böttger, D. C. Meyer, P. Paufler, S. Braun, M. Moss, H. Mai, and E. Beyer, Thin Solid Films **444**, 165 (2003).
[15]T. Tsarfati, E. Zoethout, R. van de Kruijs, and F. Bijkerk, J. Appl. Phys. **105**, 104305 (2009).
[16]M. Gorgoi, S. Svensson, F. Schäfers, G. Öhrwall, M. Mertin, P. Bressler, O. Karis, H. Siegbahn, A. Sandell, H. Rensmo, W. Doherty, C. Jung, W. Braun, and W. Eberhardt, Nucl. Instrum. Methods Phys. Res. A **601**, 48 (2009).
[17]F. Schaefers, M. Mertin, and M. Gorgoi, Rev. Sci. Instrum. **78**, 123102 (2007).
[18]The Si-oxide peak in Fig. 4 has actually increased due to the annealing treatment. This is attributed to postannealing exposure to the ambient. A rougher (see Fig. 8) and possibly more open structure are probable causes of the increased degree of oxidation.
[19]W. A. Brainard and D. R. Wheeler, J. Vac. Sci. Technol. **15**, 1800 (1978).
[20]W. Lisowski, E. G. Keim, and M. Smithers, Appl. Surf. Sci. **189**, 148 (2002).
[21]I. Kaur, Y. Mishin, and M. Gust, *Fundamentals of Grain and Interphase Boundary Diffusion* (Wiley, New York, 1995), p. 528.
[22]A. Patelli, J. Ravagnan, V. Rigato, G. Salmaso, D. Silvestrini, E. Bontempi, and L. E. Depero, Appl. Surf. Sci. **238**, 262 (2004).

Downloaded 21 Dec 2010 to 130.89.85.158. Redistribution subject to AIP license or copyright; see http://jap.aip.org/about/rights_and_permissions